

[An enhanced LSPR fiber-optic nanoprobe for ultrasensitive detection of protein biomarkers](#)

By: Mollye Sanders, Yongbin Lin, [Jianjun Wei](#), Taylor Bono, and Robert G. Lindquist

M. Sanders, Y. Lin, J. Wei, T. Bono, R. Lindquist, An enhanced LSPR fiber-optic nanoprobe for ultrasensitive detection of protein biomarkers, *Biosensors and Bioelectronics*, **2014**, 61, 95-101. <https://doi.org/10.1016/j.bios.2014.05.009>



This work is licensed under a [Creative Commons Attribution-NonCommercial-NoDerivatives 4.0 International License](#).

***© 2014 Elsevier B.V. Reprinted with permission. This version of the document is not the version of record. Figures and/or pictures may be missing from this format of the document. ***

Abstract:

A miniaturized, localized surface plasmon resonance (LSPR)-coupled fiber-optic (FO) nanoprobe is reported as a biosensor that is capable of label-free, sensitive detection of a cancer protein biomarker, free prostate specific antigen (f-PSA). The biosensor is based on the LSPR at the reusable dielectric-metallic hybrid interface with a robust, gold nano-disk array at the fiber end facet that is directly fabricated using EBL and metal lift-off process. The f-PSA has been detected with a mouse anti-human PSA monoclonal antibody (mAb) as a specific receptor linked with a self-assembled monolayer at the LSPR-FO facet surfaces. Experimental investigation and data analysis found near field refractive index (RI) sensitivity at ~ 226 nm/RIU with current LSPR-FO nanoprobe, and demonstrated the lowest limit of detection (LOD) at 100 fg/mL (~ 3 fM) of f-PSA in PBS solutions. The control experimentation using 5 mg/mL bovine serum albumin in PBS and nonspecific surface test shows the excellent specificity and selectivity in the detection of f-PSA in PBS. These results present important progress towards a miniaturized, multifunctional fiber-optic technology that integrates informational communication and sensing function for developing a high performance, label-free, point-of-care (POC) device.

Keywords: Fiber optics | Protein biomarker biosensors | Nanofabrication | Au nanodisk array | Localized surface plasmon resonance | Signal transduction

Article:

1. Introduction

Fiber-optic (FO) technology has been well-developed for optical communication (Palais, 2004); and the FO-based sensing technology has been existing as a powerful, analytical tool for a wide spectrum of applications (Wang and Wolfbeis, 2012, Wolfbeis, 2006, Wolfbeis, 2008), ranging from gas (Aernecke and Walt, 2009), chemical (Smythe et al., 2009), and biomolecule (Tam et al., 2009) detection. In recent years, FO technology has continued to enhance healthcare capability by providing effective and convenient lab tools in biomedical applications (Ben-David

and Gannot, 2007, Utzinger and Richards-Kortum, 2003), such as medical diagnostics (Bluestein et al., 1990) and therapeutics (Yoo et al., 2013), and in particular for use at inaccessible sites or remote monitoring. More recently, an emerging lab-on-fiber concept (Consales et al., 2012a, Consales et al., 2012b) is proposed to develop a new generation of miniaturized “lab” platform at optical fiber tip for both communication and sensing applications. In particular, the advances of surface plasmon resonance (SPR)-enhanced, refractive index (RI) sensing schemes, spectroscopic FO probe technology (Chang et al., 2012, Jeong et al., 2013, Lin et al., 2011a, Shevchenko et al., 2011) have demonstrated the ability for label-free bio-detection.

Surface plasmons (Raether, 1988) (SPs) are very sensitive to the near surface refractive index (RI) changes and well-suited to the detection of surface binding events. They have been exploited extensively in a variety of SPR-based sensors and biosensors (Homola, 2008). Particularly, the LSPR, caused by resonant SPs localized in nanosystems, has applications in detection of chemical and biological agents with single molecule sensitivity (Mayer and Hafner, 2011, Stewart et al., 2008, Valsecchi and Brolo, 2013). To date, various tailored noble metal nanoparticles (Bingham et al., 2009, Juvé et al., 2013, Lyon et al., 1998), nanograting metal film structures, such as nanoholes (Brolo et al., 2004, Im et al., 2009, Im et al., 2012, Sharpe et al., 2008), nanorings (Kim et al., 2006, Larsson et al., 2007, Liu et al., 2011), nanoslits (Jung et al., 2006, Lee et al., 2008, Wei et al., 2010), have been successfully fabricated for LSPR sensor applications. Modulation of the nano-structures array’s optical responses by adsorbed analytes is expected to offer improved sensitivity and selectivity over conventional SPR methods.

The implementation of a LSPR-FO-based sensor by integrating the LSPR nanoprobe to communicative fiber optics may offer many advantages, especially in terms of avoiding the use of bulky optics and high-precision mechanics for angular or wavelength interrogation of metal films in contact with analytes (Mullett et al., 2000, Shevchenko et al., 2011, Wang and Wolfbeis, 2012). In order to achieve the LSPR structure at the fiber end facet, a few approaches have been pursued in the past, and progresses have been made, including random immobilization of Au or Ag nanoparticles (NPs) (Chang et al., 2012, Jeong et al., 2013, Mitsui et al., 2004), controllable fabrication of Au nanostructures, e.g. focus ion beam (FIB) milling (Dhawan et al., 2008), or a nanoskiving method (Lipomi et al., 2010), etc. Nevertheless, there is a need to develop advanced LSPR-FO biosensors that may provide high performance, e.g. enhanced stability and high RI sensitivity, and overcome unwanted doping (Fu and Bryan, 2005), or weak adhesion (Dhawan et al., 2008).

For many years, cancer has been diagnosed and treated after the cancer cells have already invaded surrounding tissues and metastasized throughout the body, resulting in low survival rates. Early detection is the key to cancer survival, particularly so for cancers of prostate, breast, cervix, mouth, larynx, colon/rectum, and skin. Biomarkers of cancers have been found to be very important tools for cancer detection and monitoring, because they serve as hallmarks for the physiological status of a cell at a given time and change during the disease process. A few technologies have been used in biomarker applications (Wulfkuhle et al., 2003), especially in the fields of genomics and proteomics for biomarker discovery and early detection, such as DNA arrays and DNA sequencing methods, enzyme-linked immunosorbent assays (ELISAs), two-dimensional polyacrylamide gel electrophoresis, mass spectrometry, proteomic pattern

diagnostics, and protein arrays. Recent advances of biomarker detection have been made in optical (fluorescence (Mukundan et al., 2009), light scattering (Liu et al., 2008), SERS (Sekhar et al., 2008), electrochemical (Mani et al., 2009, Ramgir et al., 2007, Tang et al., 2008, Yu et al., 2006), functional quartz crystal microbalance (Henne et al., 2006), microcantilevers (Baker et al., 2008) and surface plasmon resonance (SPR) (Hegnerová et al., 2009, Kumar et al., 2007, Lee et al., 2006) sensors. Harnessing the advances in biological ligand interactions, the fiber-optic technology incorporating LSPR-nanoprobe sensing may provide an alternative tool for effective biomarker diagnosis via a compact, label-free format that does not require a dedicated laboratory facility or highly trained personnel.

In this paper, we report on the progress of developing a miniaturized LSPR-FO probe and demonstration of sensitive, label-free detection of a protein cancer biomarker, free prostate-specific antigen (f-PSA). First, a low-cost lift-off process was adapted to fabricate gold nanodisk arrays at the end of tip-facet, providing a very stable, robust and clean LSPR fiber tip probe. Then, the probe was functionalized *via* a facile self-assembled monolayer (SAM) of alkanethiolates on the gold nanodisk array to attach a capture ligand, anti-PSA antibody, as a selective immunoassay for detection of the f-PSA. The reported label-free LSPR fiber biosensor may allow an alternative approach for direct discrimination of the cancer biomarkers, and potentially developing a miniaturized, point-of-care (POC) device for early disease diagnosis.

2. Materials and methods

2.1. Materials and reagents

11-Mercaptoundecanoic acid (HSC10COOH, 99%), 8-Mercapto-1-Octanol (HSC8OH, 98%), *N*-(3-dimethylaminopropyl)-*N'*-ethylcarbodiimide hydrochloride (EDC), *N*-hydroxysuccinimide (NHS), and glycine were purchased from Sigma-Aldrich (Milwaukee, WI) and used without further purification. Mouse anti-human PSA monoclonal antibody (capture mAb), human free-PSA (Cat.# 10050) and ELISA kits for CA125 were obtained from Anogen-YES Biotech Laboratories Ltd. (Mississauga, Canada). The 5 ng/mL free-PSA standard solution was used for preparation of free-PSA solutions with lower concentrations obtained using sample dilutant provided in the ELISA kit. The 5 ng/mL free-PSA standard solution was prepared in a protein matrix solution according to the World Health Organization (WHO) standard by the vendor. All solvents and other chemicals were purchased from Sigma and used without further purification. Single-mode optical fiber for 633 nm wavelength was purchased from Newport Corporation (F-SV).

2.2. Fabrication of LSPR-FO nanoprobe

In this study, a lift-off process was developed to transfer patterns at nanometer sizes, which offers advantages of minimum damage to the fiber end facet, and without expensive plasma etch step. A single-mode optical fiber for 633 nm wavelength, which has a 4.3 μm mode field diameter, a 125 μm cladding diameter and a 245 μm polymer buffer coating diameter, was used in the fabrication. The advantage of using this small core fiber is that it provides great spectral stability in the wavelength ranges of 600 nm to 750 nm, in which the resonance peaks of fabricated fiber tip LSPR sensors were typically located. The preparation of optical fiber end

facet includes stripping off the polymer buffer layer 4 cm from the end. The end face of the optical fiber was cleaved perpendicular to the fiber axis using an optical fiber cleaver. The fiber end facet was cleaned with acetone and isopropyl alcohol rinse, followed by 120 °C oven bake for 10 min. 2 nm of Cr was deposited on the fiber end face using vacuum sputtering method (Denton sputtering system) to provide a conductive layer for the EBL process, and also as an adhesive layer for Au film overlay in the later step.

The fabrication process of LSPR-FO probe can be divided into two steps. In the first step, nano-pattern was created on the fiber end face using EBL. We used a simple and unique e-beam resist coating method “dip and vibration” technique developed in our previous study to deposit ~150 nm e-beam resist (ZEP520A, Zeon Chemicals, Japan) on the fiber end facet (Lin et al., 2009, Lin et al., 2011b, Lin et al., 2010). Then an EBL based on the Nano Pattern Generation System (NPGS) and a field emission scanning electron microscope (FESEM) were used to create nanodisks array pattern on the e-beam resist on the fiber end facet. A customized fiber holder was used to hold the fiber vertically on the translational stage in the SEM chamber. The EBL voltage was set at 20 kV and the exposure dose was 70 $\mu\text{C}/\text{cm}^2$. After EBL process, the fiber tip was developed by dipping in resist developer (ZEP N50) for 1 min. The fiber tip was then rinsed in DI water and baked in the 120 °C oven for dehydration.

In the second step, the nano-pattern was transferred to the Au layer using a metal lift-off method. The deposition of 40 nm Au overlay over the nano-patterned fiber end facet was carried out by using standard thermal evaporation coating technique. The 2 nm Cr layer previously deposited as conductive layer for EBL process is now served as an adhesive layer for Au overlay. To lift-off the e-beam resist, the fiber tip was dipped in the ZEP remover for 10 min, followed by a 1-min ultrasonic bath to assist the lift-off process. The fiber tip was then rinsed in DI water and dried in the nitrogen stream. An optical microscope with 100 \times objective lens was used to check the fiber end facet to make sure that the resist layer has been completely removed. If the lift-off process was not completed, ZEP remover and ultrasonic bath may be used to further remove the e-beam resist. After the lift-off process, the fiber tip was cleaned by DI water rinse and dry in N₂ stream. Then the fiber tip was dipped into the Cr remover solution for 30 s to remove the Cr layer that was not covered by the Au nanodisks. The fiber tip was rinsed in DI water and baked in the 120 °C oven for dehydration. Finally the Au nanodisk array on fiber end face was annealed at 530 °C for 5 min and ready for next usage.

2.3. Optical measurement

In this optical setup (Fig. 1), a 2 \times 1 single mode optical fiber coupler for 633 nm wavelength is used, which has three light connection ports. In Fig. 1, port (a) and port (b) are two connections on one side of optical fiber coupler, and port (c) is connection on the opposite side. Port (a) is connected to a tungsten halogen white light source (LS-1, Ocean Optics Inc., USA.); port (b) is connected to a mini-spectrometer (Ocean Optics USB2000); and port (c) is connected to the LSPR-FO probe using a fusion splicer. The white light (450–950 nm) is launched from port (a), propagated to port (c), and reflected from the end facet with the Au nanodisks arrays. The reflection light propagated to port (b), where the spectrum of the reflection light is measured by the mini-spectrometer, which is connected to a computer for data acquisition and processing.

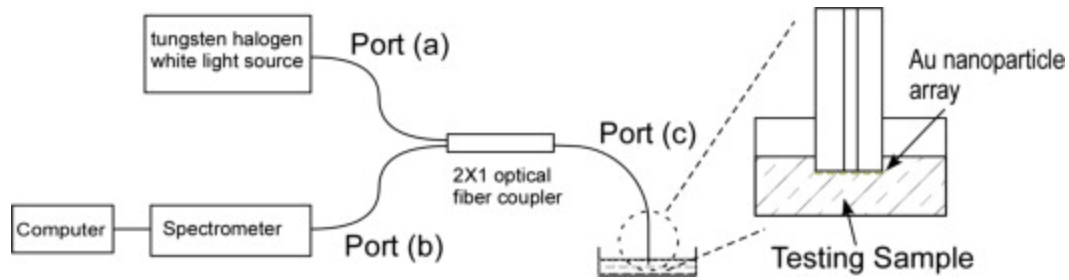


Fig. 1. Optical setup for the fiber tip LSPR sensor based on reflection spectrum measurement.

Before starting the experiment, the sensor tip must be cleaned of any impurities or other contaminants. The sensor tip is rinsed with ethanol to clean the tip. A baseline wavelength is achieved if the sensor tip returns to this wavelength three times after being washed in deionized water. If the tip spectra do not return to this line, acetone and isopropyl alcohol may be used to further clean the tip of lingering impurities.

In order to get the LSPR spectrum response due to Au nanostructures on the fiber end facet, a reference spectrum and a dark spectrum need to be recorded. The reference spectrum was acquired with no fiber LSPR probe on port (c), and the fiber end face of port (c) was perpendicularly cleaved. The dark spectrum was obtained by turning off both the tungsten halogen light source and room light. The measured reflection spectra (M_λ) of the fiber tip sensor probe was obtained by the equation:

$$M_\lambda = (S_\lambda - D_\lambda)/(R_\lambda - D_\lambda) \times 100\% \quad (1)$$

In Eq. (1), S_λ is the sample intensity, D_λ is the dark intensity, and R_λ is the reference intensity at wavelength λ .

2.4. Functionalization of the LSPR-FO nanoprobe

The immobilization of mAb at the LSPR-FO sensor surface is similar to a procedure previously reported (Zhang et al., 2012). Briefly, the cleaned fiber tip was first incubated in a mixture of 1 mM HSC10COOH and HSC8OH with mole ratio 1:5 in absolute ethanol solution for 1 h. The self-assembled monolayer (SAM) tethered with carboxylic acid groups then was activated by incubation in a pH 7.0, 10 mM phosphate buffer solution containing 0.5 mM of EDC/NHS, respectively for 1 h. The activated SAM was rinsed with the distilled water and immediately moved to a freshly prepared 10 mM PBS containing 10 $\mu\text{g}/\text{mL}$ of the detector mAb for 1 h incubation. The fiber probe was rinsed with the PBS and followed by dipping in a 0.2 M glycine PBS solution for 10 min in order to deactivate the remaining active sites at the SAM. The LSPR-FO sensor was ready for free-PSA binding detection.

2.5. Detection of f-PSA biomarker

Once the antibodies (mAbs) have been immobilized on the gold nanodisks fiber tip surface, the LSPR-FO sensor is ready for detection of f-PSA. During the experiments, PBS (containing 0.05% tween-20) was used as a running buffer to help minimizing the nonspecific adsorption of the f-PSA at the fiber tips. In order to test binding of PSA to the anti-PSA mAb modified

surfaces, five tenfold dilutions of a 5 ng/mL concentration of f-PSA were prepared in PBS solution for the desired concentrations. The sensor tip was placed in the f-PSA PBS for 10 min in the sequence from the lowest concentration of 50 fg/mL to measure the reflectance spectrum. After each measurement, the fiber tip was rinsed thoroughly with DI water, and dry in the air. All spectra were obtained after fiber tip was cleaned and dried in the air. Control experiments have been designed and carried out to evaluate the specificity/selectivity of the immunoassay using the LSPR-FO devices. Specifically, the binding between the detector mAb and bovine serum albumin (BSA) at concentrations of 5 mg/mL has been evaluated. We select BSA for this preliminary study, because the BSA is similar to human serum albumin. Additionally, in order to evaluate the nonspecific binding to the SAM, we tested the LSPR-FO devices modified only with the mix SAM of HSC10COOH and HSC8OH SAM without antibody attached by following the f-PSA detection process.

3. Results and discussion

3.1. Fabrication results and characterization

SEM images of a typical fabricated LSPR-FO probe are shown in Fig. 2. Fig. 2a shows the end face of the optical fiber with nine patches of nanodisk arrays. Each patch has a size of 30 μm by 30 μm , includes 75 \times 75 Au nanodisk array with 400 nm pitch. Although nine patches are constructed on the fiber end face, only the center one will be involved in biosensing, since the excitation light is highly confined in the fiber core, which has a diameter around 4 μm located at the center of the cladding. The other patches are there for monitoring the e-beam dose in the EBL process, and will not interference with the biosensing process in anyway. Fig. 2b shows the close up SEM image of Au nanodisks right after the lift-off process. The Au nanodisks appear to be circular with some edge roughness, 167.5 nm in diameter. Fig. 2c shows close up SEM image of the Au nanodisk array after annealing at 530 $^{\circ}\text{C}$ for 5 min. The diameter of Au nanodisks reduced to 156.3 nm with significantly less edge roughness.

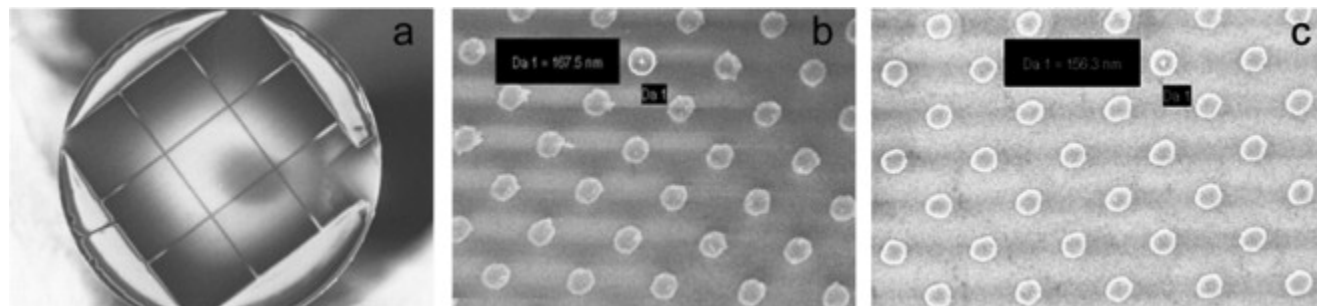


Fig. 2. Scanning electron micrographs of a gold nanodisks array on an optical fiber end facet. (a) Overview of the optical fiber end facet, (b) gold nanodisks array on the optical fiber facet after the lift-off process, and (c) gold nanodisks array on the optical fiber facet after annealing.

3.2. Nanoprobe sensitivity

The solvents used in determining the bulk RI sensitivity of the LSPR tip were acetone, methanol, ethanol, isopropyl alcohol, and water of different RIs. The sensitivity is used to determine if the sensor tip in experimentation would be perceptive enough to determine if small wavelength

shifts accurately. The LSPR-FO nanoprobe was dipped in the various solvents, and the spectra of the reflected light were recorded respectively, as shown in Fig. 3a. Please note that there is a noisy region in all spectra from ~760 nm to 800 nm, which is caused by the transmission minimum for the optical fiber coupler (single mode at 633 nm) in the same wavelength range. To determine the peak wavelength in the LSPR reflection spectrum, a Matlab program was created to fit the data to an eighth order polynomial function over a range of 80 nm, centered at the wavelength of maximum reflection in the raw data. The calculated LSPR wavelength red shifted as the RI of the solvent increased. A linear relationship between the LSPR peak wavelength and the bulk RI of the medium was obtained (Fig. 3b), with the sensitivity of 226 nm/RIU used in this study. We also investigated the light intensity based RI sensitivity. The return light intensities at the LSPR peak wavelength were plotted against the bulk RI of the media. The LSPR peak intensity is seen to be linearly proportional to the RI, and the gradient of the line is 123 per RIU. The return light intensity of a single wavelength laser can be used as a probing light for the refractive index change due to biochemistry binding events, thus eliminate the need for a broadband light source and optical spectrometer for a LSPR biosensing, which is underway. In this work, the spectral peak shifts using a white incident light were obtained for the experimentation data analysis.

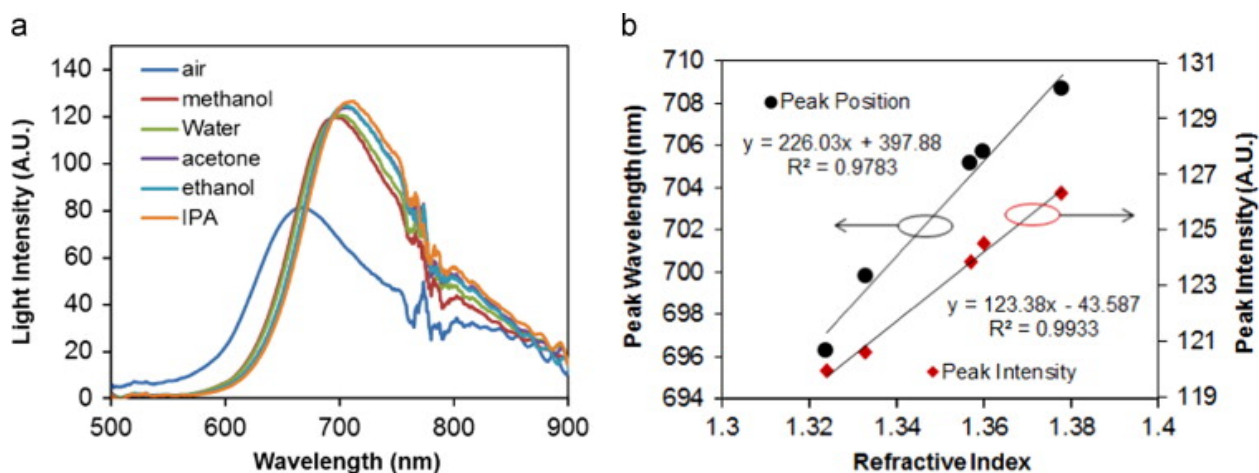


Fig. 3. (a) Measured reflection spectra for the LSPR-FO probe in various solvents. (b) Linear fit of the LSPR peak wavelengths (left axis) and LSPR peak intensity (right axis) with the index of refraction of the solvents.

3.3. Functionalization of the LSPR-FO nanoprobe

The SAM preparation from thiolated molecules at gold surfaces is well-established by the thiol-gold bond interactions (Wei et al., 2002). The SAM tethered with carboxylic acid groups is easy to be activated for biological molecule immobilization. A previously developed protocol (Zhang et al., 2012) was used to effectively immobilize the capture mAbs. With this method, the capture mAbs of f-PSA are covalently immobilized to the fiber tip facet *via* the monolayer and they are accessible for protein conjugation while maintaining native protein structure. After the antibody (mAb) attachment, the monolayer is deactivated by glycine to avoid non-specific adhesion to the active intermediates. Finally, the fiber probe was rinsed thoroughly with PBS and DI water. In such a way, the mAbs are tethered to the fiber Au nanodisks array tip surface and ready for f-PSA binding detection.

To ensure consistency in the surface functionalization with SAM and antibody attachment, the internal reflectance spectra of the Au nanodisks array FO tip interface were measured after each functionalization step. Because the thickness changes of the organic film at the LSPR surfaces will cause the effective RI changes near the surface; consequently, each step of modification at the LSPR probe surface can be detected optically by observing the LSPR wavelength shift (Jung et al., 1998). Fig. 4 shows the typical reflectance spectra of each step during the surface functionalization. The inserted image shows the smoothed spectra at the peak region by the Matlab program and the reflectance intensity is normalized to maximum peak intensity of each spectrum. The real-time monitoring of four individual LSPR-FO tips was performed, and consistent responses were obtained. In Fig. 4, one can see clear red shift after each step modification of the Au nanodisk array surface from the -SC11COOH/SC8OH SAM formation to mAb immobilization. The spectrum of the last step of glycine deactivation is almost duplicated to the step of mAb immobilization (a tiny blue shift within the spectrometer resolution 0.4 nm). This is expected because the effective RI changes depend on the amount of molecules attached to the nanostructures (Jung et al., 2006). The step-wise peak shift is originated from the near field plasmon resonance and interaction when the molecules of different dielectric constant attached to the nanostructured interface (Haes and Duyne, 2004, Haes et al., 2006, Yonzon et al., 2004).

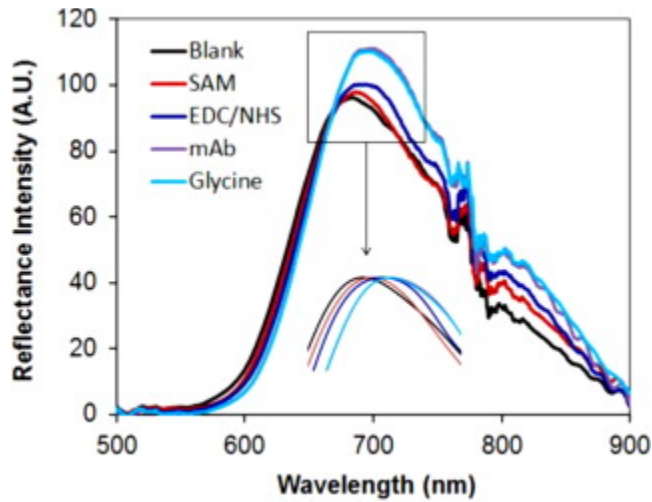


Fig. 4. Real-time reflectance spectra of the each step during the surface functionalization. Insert: spectra normalized to peak intensity to show the LSPR reflectance wavelength shifts.

Additional details of the surface modification were analyzed according to the LSPR spectral peak shift. By assuming that the total change comes from increasing the organic layer thickness, the effective dielectric constant at the modified interface can be calculated according to reference (Jung et al., 1998). From the above measured bulk RI sensitivity of 226 nm/RIU, one is able to estimate the equivalent molecular thickness of each step modification added to the precedent step according to the equation (Haemers et al., 2002, Jung et al., 1998):

$$\Delta R = m(n_{add} - n_{air})[\exp(-2d_{pre}/l_d)][1 - \exp(-2d_{pre}/l_d)] \quad (2)$$

In Eq. (2), ΔR is defined as the SPR signal response (peak shift or intensity change) after the addition of molecule layer to the precedent step modification, and m is obtained from the slope of the calibration plot (i.e. the RIU sensitivity). d_{pre} is the effective thickness of the existing layer (using 0.8 nm for the first SAM layer), l_d is the decay length of SP mode into the dielectric at the nanodisk array (two l_d value of 30 and 45 nm were used respectively for calculation according to the nanodisk dimension aspect (Chen et al., 2009)), and refractive indices of organic molecules is taken to be 1.5 (n_{add}) and that of air is 1.0 (n_{air}). According to our measured average ΔR , the calculated equivalent thickness increases of individual steps are presented in Table 1S. The increases in the layer thickness at the nanodisk tip interface are found to be ~ 0.5 nm (l_d 30 nm), or 0.73 nm (l_d 45 nm) for *O*-acylisourea intermediates after EDC/NHS, and 1.73 nm (l_d 30 nm) or 2.55 nm (l_d 45 nm) for mAb immobilization. Assuming that all of this increase comes from molecular adsorption, taking the mass weight of the mAb to be 29 kDa, and using a globular diameter of 2.6 nm (Erickson, 2009), the coverage of mAb at the LSPR sensing area is estimated to be $\sim 67\%$ (l_d 30 nm) or $\sim 98\%$ (l_d 45 nm).

The monitoring of the LSPR spectral peak shift is important to verify the success of LSPR tip functionalization with SAM and mAb. The measurement has in-situ convenience and is very effective since there is no need of any optical tag or label process. In addition, this procedure assures the complete rinse off the non-covalently bounded molecules, which is an important step to warranty the consistent measurements from individual fiber tip fabricated separately. Moreover, the quantitative analysis of surface functionalization, e.g. mAb coverage as function of RI sensitivity, is particular useful for prediction of bio-detection, and estimate of the amount of mAb immobilization at the LSPR-FO sensor area and prediction of its capability (LOD) of the target biomolecules. It will be very helpful to guide future development of reliable and reproducible bundled LSPR-FO arrays for multiplexed biomarker screening.

3.4. Cancer biomarker f-PSA detection

For demonstration, we select the FDA approved prostate cancer protein, PSA, as a model biomarker for this study. f-PSA is normally present in the blood at very low levels. The upper limit of normal concentration is much less than 4 ng/mL (Thompson et al., 2004). Hence, various concentrations of f-PSA from 50 fg/mL to 5 ng/mL in PBS solutions were used to demonstrate the capability of protein biomarker detection by the mAb functionalized LSPR-FO nanoprobe. For each concentration, the reaction time was 10 min (longer reaction time, e.g. 1–2 h, just generates insignificant further red shift, which means a dynamic equilibrium status has reached); and then the tip was rinsed in water and dried in nitrogen stream. Thereafter, the reflection spectrum was recorded in air until stable (see Fig. S1). After the set of measurements, the monolayer film was completely removed from the fiber tip by immersing it in a “piranha” solution (a mixture of 30% H₂O₂ and 98% H₂SO₄ in a 1:3 volume ratio) for 60 s, and then rinsed by water and ethanol. Typically a fiber tip probe can be reused for ~ 10 full functionalization and detection cycles. It proved that the fabricated nanodisk array at the tip facet is very stable and reusable.

Fig. 5 shows the representative reflectance spectra of f-PSA detection sensing various f-PSA concentrations from 0 ng/mL to 5 ng/mL. As expected, the primary resonance peak red shifts when the nanodisk array is exposed to f-PSA, and the red shift increases with increasing f-PSA

concentration (Jung et al., 1998, Jung et al., 2006). The smoothed curve (the inserted in Fig. 5 and spectra are normalized to peak intensity) was used to determine the peak position and the value of peak shifts at different f-PSA concentrations.

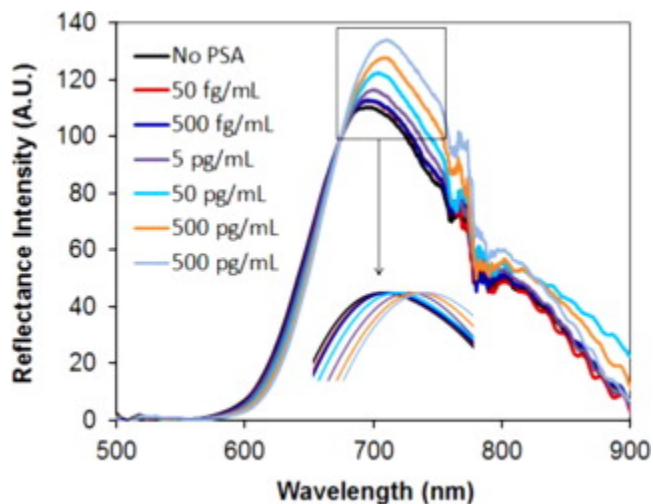


Fig. 5. The reflectance spectra of the anti-PSA mAb modified LSPR-FO tip in various of f-PSA concentration solutions. Insert: spectra are normalized to peak intensity to show the LSPR reflectance wavelength shifts.

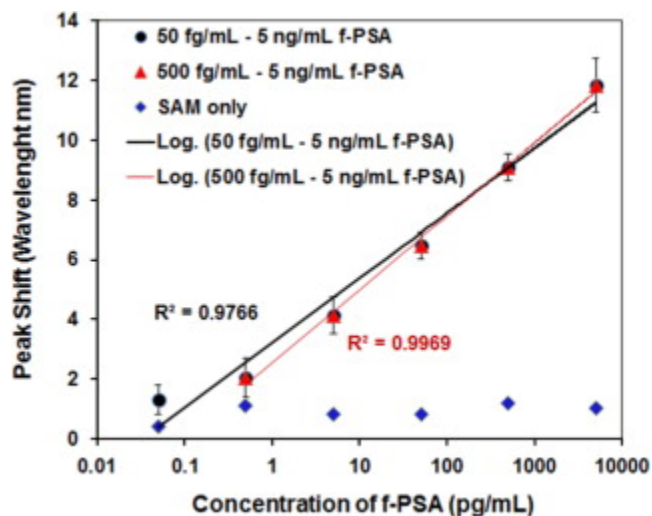


Fig. 6. Correlation of f-PSA concentration to the reflectance light of resonance peak wavelength.

3.5. Resonance peak shift

Fig. 6 shows the dependence of the wavelength peak shift on the f-PSA concentration. The peak shift for each point was obtained by averaging three measurements. The linear fit of the peak shift with logarithmic value of the f-PSA concentration gives R^2 value of 0.977 (corresponding concentration ranging 50 fg/mL to 5 ng/mL) and 0.997 (corresponding concentration ranging 500 fg/mL to 5 ng/mL), respectively, suggesting a more reliable concentration determination for the range of 500 fg/mL to 5 ng/mL. The LOD is described as the lowest concentration for clear identification of wavelength shift. The largest standard deviation of the experimental data for 3

tests is around ± 0.6 nm. A wavelength shift of twice of the largest standard deviation (1.2 nm) can be used to determine LOD of the fiber LSPR sensors, which corresponds to 100 fg/ml of f-PSA in PBS solution. To our best knowledge, this is one of the most sensitive LSPR-FO biosensors reported in the literatures (Jeong et al., 2013).

Using the peak shift ~ 11.8 nm (against to mAb tip) after exposed to 5 ng/mL f-PSA and Eq. (2), the calculated total thickness increase is 1.97 nm (with l_d 30 nm) or 2.9 nm (with l_d 45 nm), corresponding coverage of 61% or 90%, respectively (using mass weight 34 kDa and size of 3.2 nm as globular diameter), lower than the coverage of mAb, respectively. This suggests the 5 ng/mL yet not reach the highest concentration limit of detection for current LSPR-FO biosensor. Based on the coverage of mAb ($\sim 67\%$ with l_d 30 nm or $\sim 98\%$ with l_d 45 nm) and assuming fully binding to f-PSA, the calculated peak shift will be 12.85 nm (with l_d 30 nm) or 12.61 nm (with l_d 40 nm) referred to mAb layer, obtaining the predicted highest concentration of f-PSA LOD to be 15.7 ng/mL (l_d 30 nm) or 12.5 ng/mL (l_d 40 nm) by fitting to Fig. 6. We conclude that the effective LOD of current LSPR-FO biosensor is expected to be ranging from 100 fg/mL (~ 3 fM) to 15 ng/mL (~ 0.5 nM).

As a comparison, the analysis using the reflectance peak intensity is described in supplemental information (Fig. S2). The linear fit of the intensity with logarithmic value of the f-PSA concentration gives an R^2 value of 0.992 corresponding to concentration ranges of 50 fg/mL to 5 ng/mL, and 0.95 corresponding to concentration ranges of 50 fg/mL to 5 ng/mL, similar to the observation of the peak wavelength signal transduction. The data analysis by following the above described process on peak shift gives the same conclusion.

3.6. Control experimentation

Control experiments were performed to verify the specificity of mAb to f-PSA using a concentration (5 mg/mL) of BSA in PBS with the mAb LSPR-FO sensor. The peak shift of LSPR-FO with mAb in the concentration (5 mg/mL) of BSA gives ± 0.6 nm from three trials, indicating little nonspecific binding BSA to the mAb modified fiber tip. In a previous study (Zhang et al., 2012), the binding between an mAb modified Au nanostructure to rabbit IgG has been performed, which indicates excellent specificity/selectivity of the immunoassay to f-PSA. In addition, the non-specific binding of the f-PSA has been performed using the mix SAM of HSC10COOH and HSC8OH SAM (1:5) modified LSPR-FO tip in the various f-PSA concentrations. From the original reflectance spectra obtained in the f-PSA solutions (Fig. S3), one can see insignificant changes on both the peak wavelength and the light intensity with the range of 0–5 ng/mL f-PSA. Three sets of individually prepared tip were measured and the average peak shift is shown in Fig. 6 (blue diamond symbol, see raw data in Table S2). The maximum shift is about 1 nm. Since a reference of SAM-mAb modified tip was collected as the baseline for data analysis, the measured results of the f-PSA detection are consistent and effective for the bioassay. The non-specific binding of f-PSA is not an issue for the LSPR-FO biosensor. These results indicate that the nanodisk array based LSPR-FO devices, along with tailored surface modification with appropriate receptors, can be used as cancer biomarker detection with excellent sensitivity and specificity at the tested concentration range. Preliminary unpublished results for f-PSA detection in human serum have shown the promise to apply the LSPR-FO biosensor on clinical sample analysis for health care monitoring.

4. Conclusion

In summary, a multifunctional fiber-optic device that holds robust gold nanodisk arrays at the end of fiber tip facet has been investigated as a miniaturized, ultrasensitive LSPR-FO biosensor by using the internal reflectance spectrum. The Au nanodisk array probe can be cleaned and reused for surface functionalization. A consistent red shift of the primary LSPR peak was observed as the RI increases near the tip surface, validating this nanoplasmonics-based fiber-optic probe for quantitative detection of binding analyte. The bulky RI sensitivity of the LSPR-FO nanoprobe is measured as ~ 226 nm/RIU which is comparable to gold nanoparticle array-based LSPR sensors on planar substrate. The chemical and biochemical functionalization of the nanostructured tip surfaces is monitored in real-time by measuring the LSPR reflection with an incident white light at the FO tip facet interfaces. The LSPR-FO biosensor functionalized with mAb demonstrates an ultrasensitive detection of f-PSA with LOD range of 100 fg/mL (~ 3 fM) to 5 ng/mL (~ 0.15 nM) in PBS. Control experimental investigations indicate the high specificity and selectivity of the immunoassay used in the sensing of f-PSA. Moreover, the lift-off resist procedure is adaptable for fabrication of the nanodisk arrays at bundled fiber tip facets; hence it is of great potential to prepare a number of miniaturized, structurally stable multi-functional LSPR-FO biosensors for label-free, highly multiplexed sensing applications, progressing towards to develop a novel generation of lab-on-fiber point-of-care (POC) device for early diagnosis/prognosis of cancers and other diseases in health care sectors.

Acknowledgement

This work was sponsored in part by the National Science Foundation's Experimental Program to Stimulate Competitive Research (NSF EPSCoR) under grant numbers 34-21530-200-76190. J. Wei thanks the support from The Joint School of Nanoscience and Nanoengineering (JSNN).

Appendix A. Supporting information

Supplementary data associated with this article can be found in the online version at <http://dx.doi.org/10.1016/j.bios.2014.05.009>.

References

- Aernecke, M.J., Walt, D.R., 2009. Optical-fiber arrays for vapor sensing. *Sens. Actuators, B* 142 (2), 464–469.
- Baker, G.A., Desikan, R., Thundat, T., 2008. Label-free sugar detection using phenylboronic acid-functionalized piezoresistive microcantilevers. *Anal. Chem.* 80 (13), 4860–4865.
- Ben-David, M., Gannot, I., 2007. Optical fibers for biomedical applications. In: Mendez, T.F., Morse, T.F. (Eds.), *Specialty Optical Fiber Handbook*. Elsevier, Amsterdam, pp. 699–733.

- Bingham, J.M., Willets, K.A., Shah, N.C., Andrews, D.Q., Van Duyne, R.P., 2009. Localized surface plasmon resonance imaging: simultaneous single nanoparticle spectroscopy and diffusional dynamics. *J. Phys. Chem. C* 113 (39), 16839–16842.
- Bluestein, B.I., Walczak, I.M., Chen, S.-Y., 1990. Fiber optic evanescent wave immunosensors for medical diagnostics. *Trends Biotechnol.* 8, 161–168.
- Brolo, A.G., Gordon, R., Leathem, B., Kavanagh, K.L., 2004. Surface plasmon sensor based on the enhanced light transmission through arrays of nanoholes in gold films. *Langmuir* 20 (12), 4813–4815.
- Chang, T.-C., Wu, C.-C., Wang, S.-C., Chau, L.-K., Hsieh, W.-H., 2012. Using a fiber optic particle plasmon resonance biosensor to determine kinetic constants of antigen–antibody binding reaction. *Anal. Chem.* 85 (1), 245–250.
- Chen, S., Svedendahl, M., Käll, M., Gunnarsson, L., Dmitriev, A., 2009. Ultrahigh sensitivity made simple: nanoplasmonic label-free biosensing with an extremely low limit-of-detection for bacterial and cancer diagnostics. *Nanotechnology* 20 (43), 434015.
- Consales, M., Pisco, M., Cusano, A., 2012a. Lab-on-fiber technology: a new avenue for optical nanosensors. *Photonics Sens.* 2 (4), 289–314.
- Consales, M., Ricciardi, A., Crescitelli, A., Esposito, E., Cutolo, A., Cusano, A., 2012b. Lab-on-fiber technology: toward multifunctional optical nanoprobe. *ACS Nano* 6 (4), 3163–3170.
- Dhawan, A., Gerhold, M.D., Muth, J.F., 2008. Plasmonic structures based on subwavelength apertures for chemical and biological sensing applications. *IEEE Sens. J.* 8 (6), 942–950.
- Erickson, H.P., 2009. Size and shape of protein molecules at the nanometer level determined by sedimentation, gel filtration, and electron microscopy. *Biol. Proced. Online* 11, 32–51.
- Fu, Y., Bryan, N.K.A., 2005. Investigation of physical properties of quartz after focused ion beam bombardment. *Appl. Phys. B* 80 (4-5), 581–585.
- Haemers, S., Koper, G.J.M., van der Leeden, M.C., Frens, G., 2002. An alternative method to quantify surface plasmon resonance measurements of adsorption on flat surfaces. *Langmuir* 18 (6), 2069–2074.
- Haes, A., Duyne, R., 2004. A unified view of propagating and localized surface plasmon resonance biosensors. *Anal. Bioanal. Chem.* 379 (7–8), 920–930.
- Haes, A.J., Zou, S., Zhao, J., Schatz, G.C., Van Duyne, R.P., 2006. Localized surface plasmon resonance spectroscopy near molecular resonances. *J. Am. Chem. Soc.* 128 (33), 10905–10914.

Hegnerová, K., Bocková, M., Vaisocherová, H., Křištofiková, Z., Říčný, J., Řípová, D., Homola, J., 2009. Surface plasmon resonance biosensors for detection of Alzheimer disease biomarker. *Sens. Actuators, B* 139 (1), 69–73.

Henne, W.A., Doorneweerd, D.D., Lee, J., Low, P.S., Savran, C., 2006. Detection of folate binding protein with enhanced sensitivity using a functionalized quartz crystal microbalance sensor. *Anal. Chem.* 78 (14), 4880–4884.

Homola, J., 2008. Surface plasmon resonance sensors for detection of chemical and biological species. *Chem. Rev.* 108 (2), 462–493.

Im, H., Lesuffleur, A., Lindquist, N.C., Oh, S.-H., 2009. Plasmonic nanoholes in a multichannel microarray format for parallel kinetic assays and differential sensing. *Anal. Chem.* 81 (8), 2854–2859.

Im, H., Sutherland, J.N., Maynard, J.A., Oh, S.-H., 2012. Nanohole-based surface plasmon resonance instruments with improved spectral resolution quantify a broad range of antibody-ligand binding kinetics. *Anal. Chem.* 84 (4), 1941–1947.

Jeong, H.-H., Erdene, N., Park, J.-H., Jeong, D.-H., Lee, H.-Y., Lee, S.-K., 2013. Real-time label-free immunoassay of interferon-gamma and prostate-specific antigen using a fiber-optic localized surface plasmon resonance sensor. *Biosens. Bioelectron.* 39 (1), 346–351.

Jung, L.S., Campbell, C.T., Chinowsky, T.M., Mar, M.N., Yee, S.S., 1998. Quantitative interpretation of the response of surface plasmon resonance sensors to adsorbed films. *Langmuir* 14 (19), 5636–5648.

Jung, Y.S., Sun, Z., Wuenschell, J., Kim, H.K., Kaur, P., Wang, L., Waldeck, D., 2006. High-sensitivity surface plasmon resonance spectroscopy based on a metal nanoslit array. *Appl. Phys. Lett.* 88 (24) (243105–243103).

Juvé, V., Cardinal, M.F., Lombardi, A., Crut, A., Maioli, P., Pérez-Juste, J., Liz-Marzán, L.M., Del Fatti, N., Vallée, F., 2013. Size-dependent surface plasmon resonance broadening in nonspherical nanoparticles: single gold nanorods. *Nano Lett.* 13 (5), 2234–2240.

Kim, S., Jung, J.-M., Choi, D.-G., Jung, H.-T., Yang, S.-M., 2006. Patterned arrays of Au rings for localized surface plasmon resonance. *Langmuir* 22 (17), 7109–7112.

Kumar, S., Harrison, N., Richards-Kortum, R., Sokolov, K., 2007. Plasmonic nanosensors for imaging intracellular biomarkers in live cells. *Nano Lett.* 7 (5), 1338–1343.

Larsson, E.M., Alegret, J., Käll, M., Sutherland, D.S., 2007. Sensing characteristics of NIR localized surface plasmon resonances in gold nanorings for application as ultrasensitive biosensors. *Nano Lett.* 7 (5), 1256–1263.

- Lee, H.J., Nedelkov, D., Corn, R.M., 2006. Surface plasmon resonance imaging measurements of antibody arrays for the multiplexed detection of low molecular weight protein biomarkers. *Anal. Chem.* 78 (18), 6504–6510.
- Lee, K.-L., Wang, W.-S., Wei, P.-K., 2008. Sensitive label-free biosensors by using gap plasmons in gold nanoslits. *Biosens. Bioelectron.* 24 (2), 210–215.
- Lin, Y., Zou, Y., Lindquist, R.G., 2011a. A reflection-based localized surface plasmon resonance fiber-optic probe for biochemical sensing. *Biomed. Opt. Express* 2 (3), 478–484.
- Lin, Y.B., Guo, J.P., Lindquist, R.G., 2009. Demonstration of an ultra-wideband optical fiber inline polarizer with metal nano-grid on the fiber tip. *Opt. Express* 17 (20), 17849–17854.
- Lin, Y.B., Zou, Y., Lindquist, R.G., 2011b. A reflection-based localized surface plasmon resonance fiber-optic probe for biochemical sensing. *Biomed. Opt. Express* 2 (3), 478–484.
- Lin, Y.B., Zou, Y., Mo, Y.Y., Guo, J.P., Lindquist, R.G., 2010. E-beam patterned gold nanodot arrays on optical fiber tips for localized surface plasmon resonance biochemical sensing. *Sensors* 10 (10), 9397–9406.
- Lipomi, D.J., Martinez, R.V., Kats, M.A., Kang, S.H., Kim, P., Aizenberg, J., Capasso, F., Whitesides, G.M., 2010. Patterning the tips of optical fibers with metallic nanostructures using nanoskiving. *Nano Lett.* 11 (2), 632–636.
- Liu, S.-D., Yang, Z., Liu, R.-P., Li, X.-Y., 2011. High sensitivity localized surface plasmon resonance sensing using a double split nanoring cavity. *J. Phys. Chem. C* 115 (50), 24469–24477.
- Liu, X., Dai, Q., Austin, L., Coutts, J., Knowles, G., Zou, J., Chen, H., Huo, Q., 2008. A one-step homogeneous immunoassay for cancer biomarker detection using gold nanoparticle probes coupled with dynamic light scattering. *J. Am. Chem. Soc.* 130 (9), 2780–2782.
- Lyon, L.A., Musick, M.D., Natan, M.J., 1998. Colloidal Au-enhanced surface plasmon resonance immunosensing. *Anal. Chem.* 70 (24), 5177–5183.
- Mani, V., Chikkaveeraiah, B.V., Patel, V., Gutkind, J.S., Rusling, J.F., 2009. Ultrasensitive immunosensor for cancer biomarker proteins using gold nanoparticle film electrodes and multienzyme-particle amplification. *ACS Nano* 3 (3), 585–594.
- Mayer, K.M., Hafner, J.H., 2011. Localized surface plasmon resonance sensors. *Chem. Rev.* 111 (6), 3828–3857.
- Mitsui, K., Handa, Y., Kajikawa, K., 2004. Optical fiber affinity biosensor based on localized surface plasmon resonance. *Appl. Phys. Lett.* 85 (18), 4231–4233.

- Mukundan, H., Xie, H., Anderson, A.S., Grace, W.K., Shively, J.E., Swanson, B.I., 2009. Optimizing a waveguide-based sandwich immunoassay for tumor biomarkers: evaluating fluorescent labels and functional surfaces. *Bioconjugate Chem.* 20 (2), 222–230.
- Mullett, W.M., Lai, E.P.C., Yeung, J.M., 2000. Surface plasmon resonance-based immunoassays. *Methods* 22 (1), 77–91.
- Palais, J.C., 2004. *Fiber Optic Communications* (fifth ed.).
- Raether, H., 1988. *Surface Plasmons on Smooth and Rough Surfaces and on Gratings*. Springer, Berlin.
- Ramgir, N.S., Zajac, A., Sekhar, P.K., Lee, L., Zhukov, T.A., Bhansali, S., 2007. Voltammetric detection of cancer biomarkers exemplified by interleukin-10 and osteopontin with silica nanowires. *J. Phys. Chem. C* 111 (37), 13981–13987.
- Sekhar, P.K., Ramgir, N.S., Bhansali, S., 2008. Metal-decorated silica nanowires: an active surface-enhanced raman substrate for cancer biomarker detection. *J. Phys. Chem. C* 112 (6), 1729–1734.
- Sharpe, J.C., Mitchell, J.S., Lin, L., Sedoglavich, N., Blaikie, R.J., 2008. Gold nanohole array substrates as immunobiosensors. *Anal. Chem.* 80 (6), 2244–2249.
- Shevchenko, Y., Francis, T.J., Blair, D.A.D., Walsh, R., DeRosa, M.C., Albert, J., 2011. In situ biosensing with a surface plasmon resonance fiber grating aptasensor. *Anal. Chem.* 83 (18), 7027–7034.
- Smythe, E.J., Dickey, M.D., Bao, J., Whitesides, G.M., Capasso, F., 2009. Optical antenna arrays on a fiber facet for in situ surface-enhanced raman scattering detection. *Nano Lett.* 9 (3), 1132–1138.
- Stewart, M.E., Anderton, C.R., Thompson, L.B., Maria, J., Gray, S.K., Rogers, J.A., Nuzzo, R.G., 2008. Nanostructured plasmonic sensors. *Chem. Rev.* 108 (2), 494–521.
- Tam, J.M., Song, L., Walt, D.R., 2009. DNA detection on ultrahigh-density optical fiber-based nanoarrays. *Biosens. Bioelectron.* 24 (8), 2488–2493.
- Tang, D., Yuan, R., Chai, Y., 2008. Ultrasensitive electrochemical immunosensor for clinical immunoassay using thionine-doped magnetic gold nanospheres as labels and horseradish peroxidase as enhancer. *Anal. Chem.* 80 (5), 1582–1588.
- Thompson, I.M., Pauler, D.K., Goodman, P.J., Tangen, C.M., Lucia, M.S., Parnes, H.L., Minasian, L.M., Ford, L.G., Lippman, S.M., Crawford, E.D., Crowley, J.J., Coltman, C.A., 2004. Prevalence of prostate cancer among men with a prostate-specific antigen level ≥ 4.0 ng/mL. *N. Engl. J. Med.* 350 (22), 2239–2246.

- Utzing, U., Richards-Kortum, R.R., 2003. Fiber optic probes for biomedical optical spectroscopy. *J. Biomed. Opt.* 8 (1), 121–147.
- Valsecchi, C., Brolo, A.G., 2013. Periodic metallic nanostructures as plasmonic chemical sensors. *Langmuir* 29 (19), 5638–5649.
- Wang, X.-D., Wolfbeis, O.S., 2012. Fiber-optic chemical sensors and biosensors (2008–2012). *Anal. Chem.* 85 (2), 487–508.
- Wei, J., Liu, H., Dick, A.R., Yamamoto, H., He, Y., Waldeck, D.H., 2002. Direct wiring of cytochrome c's heme unit to an electrode: electrochemical studies. *J. Am. Chem. Soc.* 124 (32), 9591–9599.
- Wei, J., Singhal, S., Kofke, M., Waldeck, D.H., 2010. Transmission SPR of gold nanoslit array and ultrasensitive detection of a retinol binding protein. In: *Bioinformatics and Biomedical Engineering (iCBBE), 2010 Fourth International Conference on*, pp. 1-4. IEEE Xplore.
- Wolfbeis, O.S., 2006. Fiber-optic chemical sensors and biosensors. *Anal. Chem.* 78 (12), 3859–3874.
- Wolfbeis, O.S., 2008. Fiber-optic chemical sensors and biosensors. *Anal. Chem.* 80 (12), 4269–4283.
- Wulfkuhle, J.D., Liotta, L.A., Petricoin, E.F., 2003. Proteomic applications for the early detection of cancer. *Nat. Rev. Cancer* 3 (4), 267–275.
- Yonzon, C.R., Jeoung, E., Zou, S., Schatz, G.C., Mrksich, M., Van Duyne, R.P., 2004. A comparative analysis of localized and propagating surface plasmon resonance sensors: the binding of concanavalin a to a monosaccharide functionalized self-assembled monolayer. *J. Am. Chem. Soc.* 126 (39), 12669–12676.
- Yoo, W., Seo, J., Shin, S., Han, K.-T., Jeon, D., Jang, K., Sim, H., Lee, B., Park, J.-Y., 2013. Measurements of entrance surface dose using a fiber-optic dosimeter in diagnostic radiology. *Opt. Rev.* 20 (2), 173–177.
- Yu, X., Munge, B., Patel, V., Jensen, G., Bhirde, A., Gong, J.D., Kim, S.N., Gillespie, J., Gutkind, J.S., Papadimitrakopoulos, F., Rusling, J.F., 2006. Carbon nanotube amplification strategies for highly sensitive immunodetection of cancer biomarkers. *J. Am. Chem. Soc.* 128 (34), 11199–11205.
- Zhang, T., He, Y., Wei, J., Que, L., 2012. Nanostructured optical microchips for cancer biomarker detection. *Biosens. Bioelectron.* 38 (1), 382–388.